Journal Pre-proofs

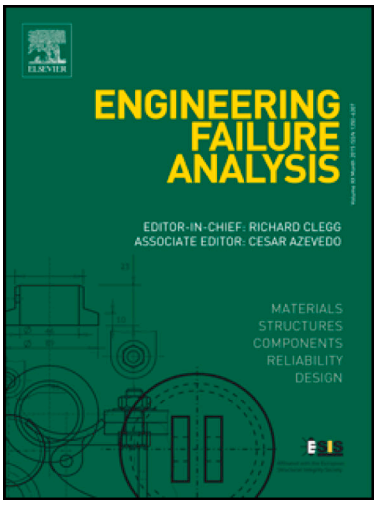

Operating conditions leading to crack propagation in turbine blades of tidal barrages. Influence of head and operating mode

Yongyao Luo, Alexandre Presas, Zhengwei Wang, Yexiang Xiao, Haoping Wang, Xiaoyi Jiang

PII: S1350-6307(19)30342-5
DOI: https://doi.org/10.1016/j.engfailanal.2019.104254
Reference: EFA 104254

To appear in: *Engineering Failure Analysis*

Received Date: 6 March 2019
Revised Date: 2 October 2019
Accepted Date: 4 November 2019

Please cite this article as: Luo, Y., Presas, A., Wang, Z., Xiao, Y., Wang, H., Jiang, X., Operating conditions leading to crack propagation in turbine blades of tidal barrages. Influence of head and operating mode, *Engineering Failure Analysis* (2019), doi: https://doi.org/10.1016/j.engfailanal.2019.104254

Operating conditions leading to crack propagation in turbine blades of tidal barrages. Influence of head and operating mode

Yongyao Luo[1], Alexandre Presas[1], Zhengwei Wang[1]*, Yexiang Xiao[1], Haoping Wang[2], Xiaoyi Jiang[2]

1. *Department of Energy and Power Engineering, Tsinghua University, Beijing, China, 100084*
2. *Jiangxia Tidal Test Power Station, Wenling, Zhejiang, China, 317528*

Abstract

Tidal energy systems and specifically tidal barrages are renewable energy systems, that use the potential energy of tides to produce electricity. Actually, there are few tidal power stations operating, although recent studies show the potentiality of installing new units in a recent future due to the constant improvement of the technology related. As in other conventional hydropower systems, the runner is one of the critical components of the unit as it has to withstand an extreme wide range of relative head and two main operating modes (ebb and flood). Therefore, fatigue problems and undesirable failures are more likely to occur. Based on the analysis of a crack found in one of the blades of a prototype, this paper analyzes and discusses under which operating conditions the runner is more likely to suffer from fatigue problems. CFD and FEM simulation models have been used to determine the stress hotspots, which approximate very well the point where the real crack was initiated. Based on a probabilistic approach of an existing initial defect or flaw, the reliability of the blades, or the probability of not growing a crack and therefore last an infinite life, has been calculated for a wide range of operating conditions. While fatigue problems have been deeply discussed and analyzed in conventional turbines, the flow excitation characteristics in these units exhibit important differences and therefore the discussion and results provided in this paper could be useful for future designs and fatigue analyses of tidal turbines.

Keywords: tidal energy; dynamic stress; fatigue; bulb turbine

1. Introduction

Tidal energy is a renewable energy system that uses the potential energy of tides and convert it into electricity. According to recent studies, although tidal energy is not widely used yet, it has a great potential for a near future to become a more important renewable energy source[1]. With respect to wind and solar power, tides are much more predictable which is extremely important for the stability of the grid. The operating principle is similar to that for hydroelectric generation, as the mechanical energy of water is converted into electricity. Types of tidal power systems can be classified in tidal turbines, tidal fences and tidal barrages, being the last the most efficient one. In tidal barrages, a dam (barrage) is built across an estuary or coastal inlet to accumulate potential energy of tides (tides have a cycle with two maximums every 24 hours, 50 minutes and 28 seconds[2]), which can be transformed to

* Corresponding author E-mail: wzw@tsinghua.edu.cn. Tel: +8610 62791262.

electricity by means of a turbine. When the tide rises, water moves towards the coast which is known as flood current, when the tide recedes, the water current moving away is called ebb current. Consequently, tidal barrages can theoretically use both type of currents to generate electricity. The tidal energy is approximately proportional to the square of the tidal range and the area of the water trapped in the barrage. There are currently five major tidal power plants in the world, the La Rance tidal power plant on the river Rance in Brittany, France [3]; Kislaya Guba tidal in Russia [4]; Annapolis in the Bay of Fundy, Canada[5]; Jiangxia in China [6]; Sihwa in the Sihwa Bay, South Korea, which is the world's largest tidal power plant so far [7]. The La Rance and Jiangxia tidal power plants use both the flood and ebb phases of the tide to generate electricity so they have shorter periods of non-generation. The feasibility of new tidal power utilization in different countries has been also analyzed[8-12].

The bulb tubular turbine has been generally used in tidal power plants. As in other more conventional reaction hydro turbines (Francis and Kaplan turbines), it is of paramount importance to carefully analyze and assess possible fatigue problems. In reaction turbines, such studies are a complex Fluid-Structure Interaction problem, where two parts have to be considered. On one side, the characteristics of the flow excitation caused by the water passing through the turbine have to be determined. On the other side, the dynamic response of the structure, which is also greatly affected by the flow (added mass and added damping) has to be considered as well.

Many studies have been focused on the numerical analysis of the flow excitation of Kaplan and specially Francis Turbines. For example, in Kaplan Turbines, the fracture appeared in the piston rod of the runner could be explained by means of a CFD simulation model [13, 14]. Liu et al. [15] predicted the flow characteristics in a reduced scale model Kaplan turbine by means of CFD simulations, which agree with the experimental observations in terms of frequencies and amplitudes. For Francis Turbines there are plenty of CFD studies considering the different operating regimes. Examples of CFD analysis at speed no load condition[16-18] , deep part load[19], part load with vortex rope [20, 21] and full load conditions[22, 23] can be found in the aforementioned references. Generally, periodical phenomena in Francis and Kaplan Turbines, such as the Rotor Stator Interaction (RSI) or the vortex rope can be well captured with actual numerical CFD methods. The main challenge is still to properly simulate the stochastic part of the flow excitations, which is predominant at speed no load and deep part load conditions.

When analyzing fatigue problems in turbine runners, the next step is to transpose the pressure fluctuations obtained with the CFD simulation model in the structural model, so that mean and dynamic stresses can be calculated. Therefore, the accuracy of the mean and dynamic stresses obtained strongly depends on the accuracy of the CFD model. This procedure has been extensively performed for Kaplan and Francis Turbines. In Kaplan turbine runners, Luo et al.[14] and Zhou et al. [24] numerically obtained the static and dynamic stresses on the blades of the turbine. Much more studies are found in Francis turbines. For example Xiao et al. [25] concluded that off-design conditions lead to crack propagations in the runner. Also Egusquiza et al. [26] applied the RSI characteristic to determine the stress hotspot in a pump turbine prototype, which could explain the damage found. More recently Huang et al.[27], Seidel et al.[28], Monette et al.[29], Duparchy et al. [30] have shown a good agreement between numerical predictions and experimental measurements of stresses, performed with strain gauges, especially for full load conditions, where the RSI dominates. Regarding low head bidirectional bulb turbines, which are used in tidal barrages and which are the focus of the present study, no papers have been found where dynamic stresses are predicted combining CFD and FEM simulation models, although the same generic numerical methods used for conventional turbines can be employed.

Once the static and dynamic stresses are obtained, fatigue life assessment of the turbine runner or associated components can be performed using different fatigue models. Some researches use the Miner's rule to estimate the relative damage of every operating condition[27-29]. Adapted versions of the Paris Law [31, 32] have been successfully used to predict the number of cycles to fracture. Finally, the reliability of the machine, defined as the probability of not propagating a crack, has been recently defined by Gagnon et al. [33-35] using the limits defined by the Kitagawa diagram. Such types of fatigue assessments are still yet not typical in tidal turbines, maybe because the limited number of installed units compared to Francis and Kaplan turbines.

In this paper, a comprehensive fatigue analysis of the turbine units in one of the most important operating tidal barrages at the present, has been performed with the aim to determine which operating conditions are more prone to grow a crack on the turbine blade. A numerical CFD model including gravity effects has been used to determine the flow pressure pulsations. These have been used in an FEM structural model to determine the static (mean) and dynamic stresses. Based on previous fatigue studies with the material ASTM A743CA6NM steel, which is a common one in hydraulic runners and also used in the analyzed turbine, the limit of fatigue considering the effect of mean stresses has been obtained. Finally, considering a probabilistic model for a small initial flaw or defect, the reliability of the blades, defined as the probability of not propagating a crack (infinite fatigue life), has been determined for the unit operating in ebb and flood mode and for a wide range of net heads.

2. Numerical simulation model

2.1 Unit description and damages found

The turbine unit analyzed in this paper works in one of the two bidirectional tidal barrages, operating at the present. Every unit has a power of 700 kW with a rated head of 3 meters, rated flow rate of 32 m^3/s for ebb mode and 28 m^3/s for flood mode with a rotating speed of 125 rpm. The runner is a horizontal shaft low head bulb turbine with 4 blades and 16 guide vanes. The diameter of the runner is 2.5 m. The blade profile is an "S" type to achieve high efficiency for both flood and ebb turbine modes. As mentioned before, the particularity of these units is that they are bidirectional, i.e. the flood and the ebb currents can be used to generate electricity. An overview of this unit can be seen in **Figure 1**.

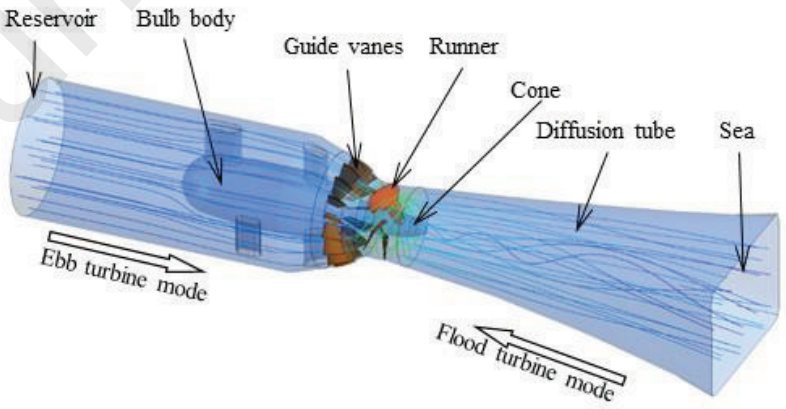

***Figure 1**: Main components of the bulb turbine unit. Ebb and flood current direction*

These turbines work with an extreme variation of the relative head compared to conventional hydro turbines. As a comparison example, for the analyzed unit in this paper, the ratio of head variation (H_{max}/H_{min}) is 4.5, while for the conventional Francis Unit recently analyzed in the HYPERBOLE project this ratio is 1.38 [36]. These variations in head lead to important variations in stress characteristic of the machine and therefore the purpose is to determine under which operating conditions cracks are more prone to be developed. This has to be determined for the unit working in the ebb mode and in the flood mode (**Figure 1**). Therefore, static and dynamic stresses on the blades have to be calculated for the different operating conditions. In the past, during overhaul inspections different cracks on the blades have been found as the shown one in **Figure 2**.

***Figure 2**: Crack found in one blade of a bulb turbine unit*

2.2 CFD simulation model

In order to determine the stresses and analyze the origin of the cracks, first the pressure fluctuations originated by the flow, which acts on the turbine blades, have to be analyzed. As in past studies mentioned before, the pressure fluctuations are determined by means of a CFD model. For the present study, the calculations have been performed using ANSYS software.

The flow path is meshed with an unstructured hybrid mesh of hexahedral and tetrahedral elements, as shown in Figure 3. The water is assumed to be incompressible. The time-dependent Reynolds average (RANS) Navier-Stokes equations and the SST k-ω (k-ω shear stress transport) turbulence model [37] are used as the governing equations of the flow field through the bulb turbine.

In the simulations, the runner zone rotates at 125 rpm (rotating speed of the machine) while the other zones remain stationary. The interfaces between the runner and the guide vanes, as well as the diffusion tube uses a transient rotor-stator frame change/mixing model. Static pressure conditions are set at the inlet and outlet boundaries according to the water level for each operating condition. For these simulations the gravity force has been considered due to the high relative static pressure variation at the inlet and outlet section (Figure 4). As can be seen in this figure the variation of the pressure between the upper and the bottom part of the inlet and of the outlet is very high and relevant for the flow analysis in horizontal low head turbines. The transient calculation uses a time step of 0.0048 s (i.e., 1% of the runner rotational period), which is small enough to capture the main pressure fluctuation frequencies, such as the rotational frequency and the blade passing frequency.

Figure 3: *Mesh along the flow path*

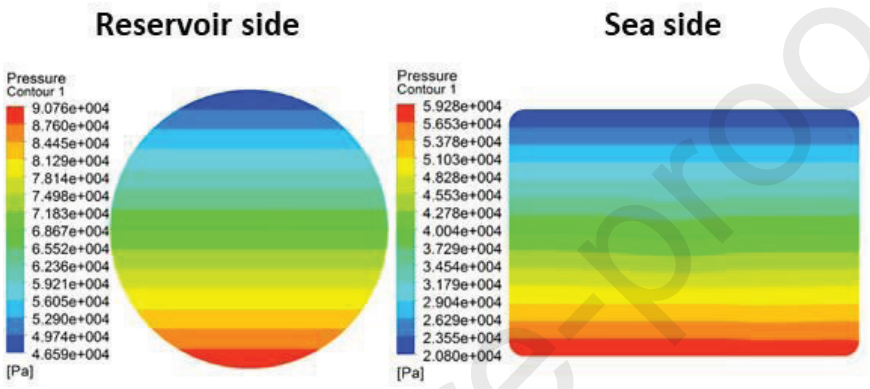

Figure 4: *Inlet and outlet boundary conditions*

2.3 FEM simulation model

Once the flow excitation is obtained, the resulting pressure pulsation on the discretized points of the blades are transferred to the Finite Element Model (FEM), so that the static and dynamic stresses can be obtained. On the blades surfaces, both the CFD and the FEM model share the same nodes, as shown in Figure 5. In order to transfer the pressure fluctuation into the FEM model at each time step, a specific developed code is used.

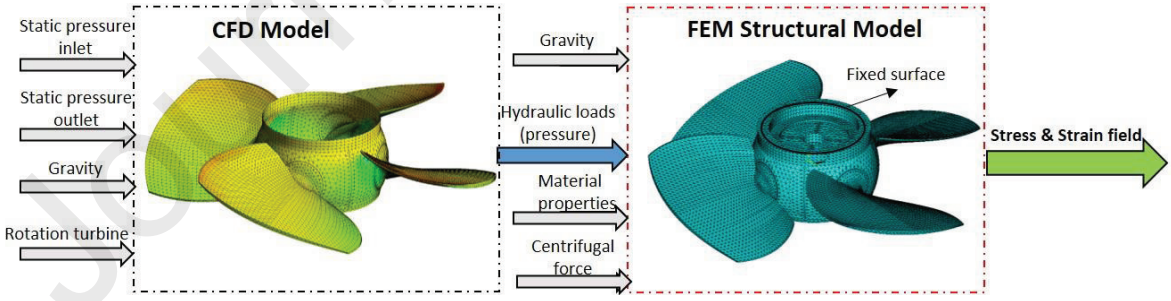

Figure 5: *Flowchart of the simulation process*

The structural generic equilibrium equation to determine the structural displacement field is as following:

$$[M]\{\ddot{u}\} + [C]\{\dot{u}\} + [K]\{u\} = \{F\} \quad (1)$$

Here $[M]$, $[C]$, $[K]$ are the mass, damping and stiffness matrices, $\{u\}$, $\{\dot{u}\}$, $\{\ddot{u}\}$ are the nodal displacement, velocity and acceleration vectors, and $\{F\}$ is the nodal load vector including gravitational

forces, centrifugal forces and the hydraulic pressures obtained from the flow simulation. The equation is then discretized and solved with the Newmark method, which is usually used for implicit transient analyses [38] (as the pressure pulsation of the flow modifies $\{F\}$ every time step). Once Eq.(1) is numerically solved, the nodal displacements $\{u\}$ are obtained at the discretized points. Then, the strain and stress fields can be easily calculated with the use of ANSYS.

3. Pressure pulsation and dynamic stresses on the blades

3.1 Operating conditions simulated

To cover the full operating range of the machine, seven different heads in the full head range of the machine (1.2m- 5.5m) have been simulated for the ebb and flood mode. The parameters of these conditions are listed in Table 1. The turbine operates in the on-cam mode for the ebb turbine mode (changing the position of the guide vane angle and blade angle). In this mode the guide vane and blade are adjusted to one specific angle for every particular head in order to optimize the efficiency of the unit (see Table 1). For the flood turbine mode, as the guide vanes are located downstream of the turbine, their role is less important and therefore the angle is kept at 110°, which gives the best overall efficiency in this mode.

Table 1: *Operating conditions simulated*

Net head H（m）	Ebb turbine mode			Flood turbine mode		
	Flow rate (m^3/s)	Guide vane angle (°)	Blade angle (°)	Flow rate (m^3/s)	Guide vane angle (°)	Blade angle (°)
1.2	19.0	75	17.5	21.5	110	17.5
1.5	19.1	70	17.5	22.0	110	17.5
2.0	19.3	66	17.5	22.8	110	17.5
2.5	19.6	62.5	17.5	23.5	110	17.5
3.0	19.9	60	17.5	24.1	110	17.5
4.0	20.5	55	17.5	25.5	110	17.5
5.5	21.1	52	17.5	27.4	110	17.5

3.2 Pressure pulsations

The temporary signal of the pressure is stored for two points in both sides of the blade. RP (Runner Pressure side) is on the pressure side when the turbine works in ebb mode and RS (Runner suction side) is on the suction side also for the ebb mode (Figure 6). Note that the pressure and suction side are interchanged in flood mode.

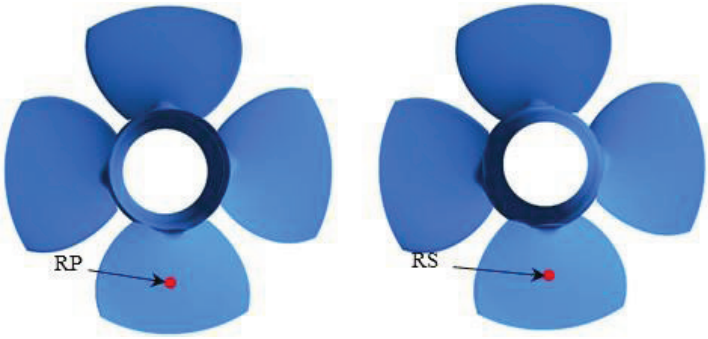

***Figure 6**: Location of the monitor points on the pressure side (RP) and suction side (RS) in ebb mode*

The pressure contour over the blades shown in Figure 7, explain the importance of the submergence level of every relative point (static pressure). One blade is intentionally left without pressure contour in order to easily follow the evolution of one turn for the pressure and the suction side. A blade in the lower position has a high pressure level. In half turn of the machine, the same blade is in an upper position and as the submergence level is less, the pressure is lower. This effect is especially important in very low head horizontal machines with a relative high diameter (D/H≈0.83 for the nominal head in this case), while for more conventional turbines (vertical machines with high head) such effects do not play an important role.

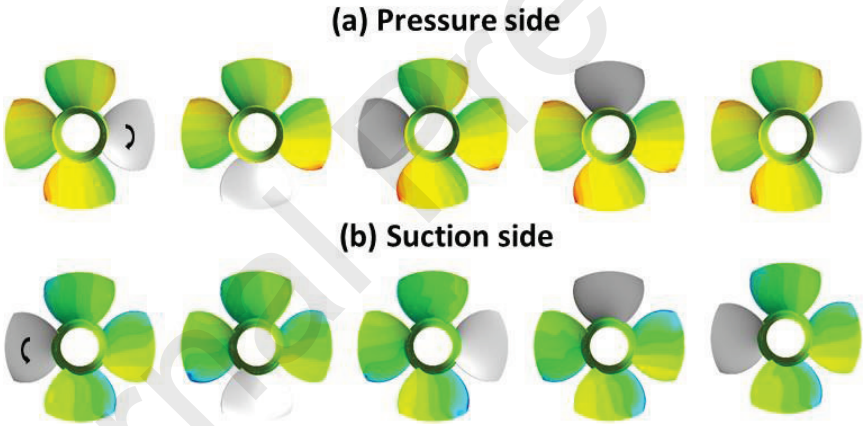

***Figure 7**: Pressure distributions on the blade at different times for the ebb turbine mode ($\Delta t = T/4$)*

Such evolution can be also clearly appreciated, when analyzing the time signals of the monitored points RP and RS (**Figure 8**). The time has been normalized with the rotating period of the machine, so that one unit corresponds to one complete turn. Non other clear components besides the rotating frequency can be observed in the time signals. It has been also checked that the first natural frequency of the submerged turbine is much higher than the excitation produced by the rotation of the unit and therefore for this unit the risk of a structural resonance is very limited.

Note that in Ebb mode the pressure corresponding to RP is higher than for RS and the opposite for the flood mode as the pressure and suction side are interchanged within two modes. The absolute difference between both points increases with increasing head for the two operating modes, as the net force on the blades is higher. The mean level of RP in ebb mode and RS in flood mode increases for increasing head due to the column of water above.

The dynamic component is clearly dominated by the rotation of the blade. In the lower position the

pressure is higher and in the higher position the pressure is minimum, which has been also seen in **Figure 7**. In the ebb mode at low heads (**Figure 8**a) a turbulence of the secondary flow is appreciated in the RS point, which distorts the perfectly cyclic shape observed in the other patterns.

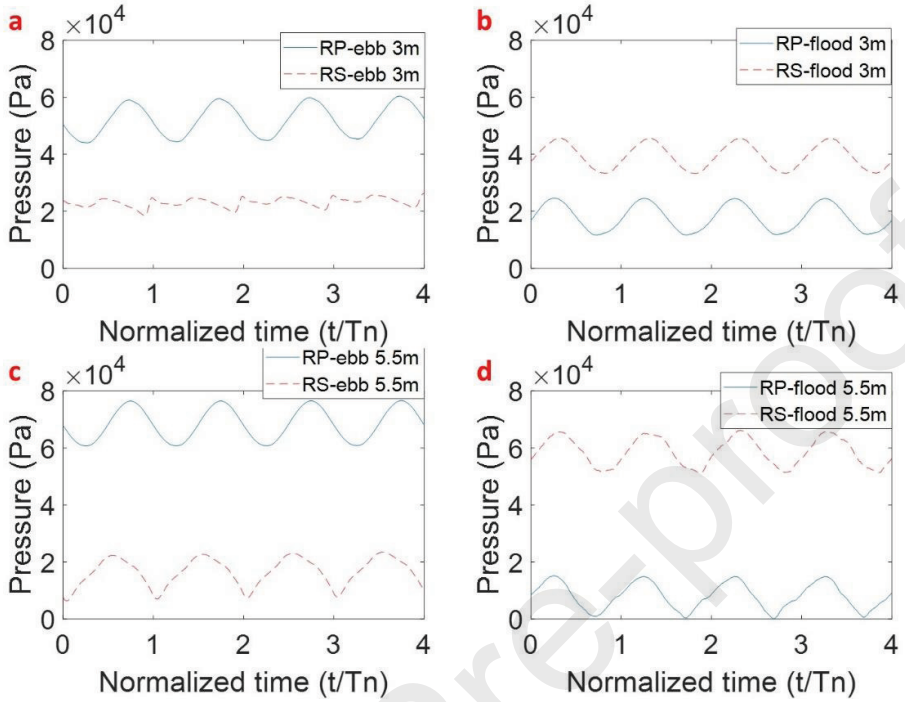

Figure 8: *Time signals of the monitored points RP and RS. a) Ebb mode and 3 m head b) Flood mode and 3 m head. c) Ebb mode and 5.5 m head d) Flood mode and 5.5 m head*

The mean and fluctuating pressure is represented as function of the head in **Figure 9**. Regarding the mean values, as commented for the previous figure, RP in ebb mode and RS in flood mode increase with increasing head. As the force on the blade increases with the head, the absolute pressure difference between the two monitoring point increases with increasing head. The alternate values which depend on the rotation of the runner and therefore on the variation of the submergence level of RP and RS are approximately constant for increasing head. Only RS in ebb mode, which is also influenced by the turbulence on the outlet, shows lower values for lower head where the turbulence at the outlet is more important (also shown in **Figure 8**). For higher heads this turbulence has less influence and the alternate pressure slightly increases.

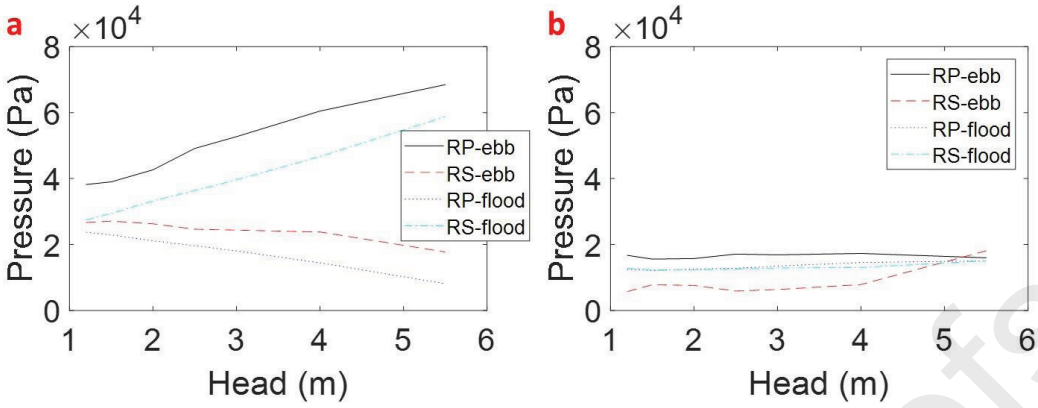

Figure 9: *a) Mean and b)fluctuating pressure as function of the head for the ebb and flood mode*

3.3 Stress distribution

The pressure field obtained with the CFD is applied on the structural Finite Element model. The stress distributions on the blade for the ebb and flood modes are shown in Figure 10 a and Figure 10 b respectively. Note that in both cases the maximum stress is located on the root of the blade. Note also that in Figure 10a the runner is viewed from the reservoir side to the sea side (Figure 1) while in Figure 10b the runner is viewed in the opposite direction (the cone is not considered in the FEM model). A crack found in one of the real bulb turbine prototypes (Figure 10c) shows the agreement between the crack initiation point and the stress hotspot predicted.

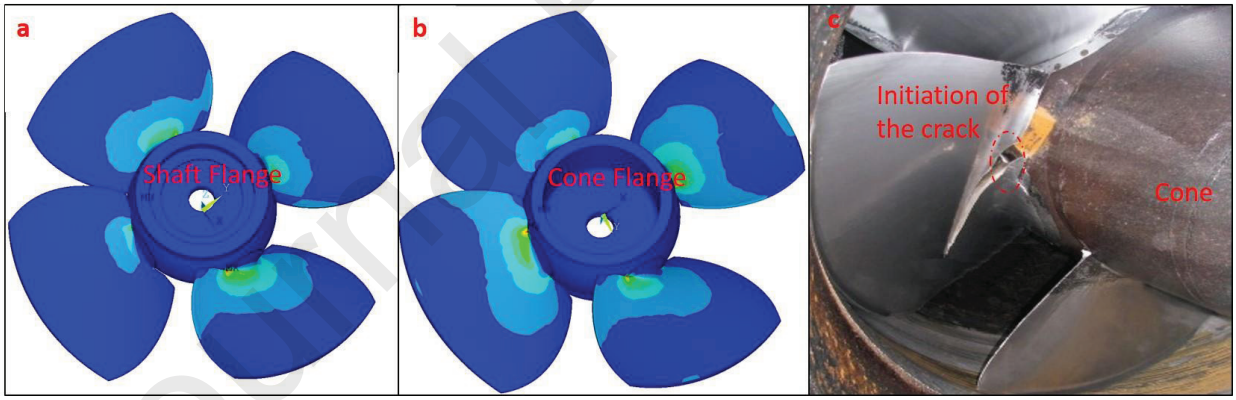

Figure 10*: Stress distribution for a) Ebb mode and b) Flood mode. c) Real crack found*

The behavior of the stress fluctuations on the hotspot (**Figure 11**) can be easily explained considering the characteristic of the pressure fluctuations (**Figure 8**). These are dominated by one single frequency, namely the rotating frequency of the machine, which also dominates the pressure field. It can be seen that increasing the head increases the mean stress, as the absolute difference in pressure between RP and RS increases (**Figure 9**a). The alternate stress remains approximately constant independently of the head, being larger for the Ebb mode, similar as by the alternate pressure (**Figure 9**b). In the same way as is done in **Figure 10** for the pressure field, **Figure 12** represents the evolution of the mean and alternate stress with the head for the Ebb and Flood mode, showing the behavior above-mentioned. It has to be noticed, that for the ebb mode the mean stresses are slightly lower than for the Flood mode,

while the alternate stresses are slightly higher. Besides the mean and the alternate stress, the ratio *R* defined as in Eq. (2) is represented. For $-1 < \mathrm{R} < 1$ the stress mean value is positive, tending to infinite for $\mathrm{R} \to 1$, which implies a mean tensile stress.

$$\mathrm{R} = \frac{\sigma_{min}}{\sigma_{max}} \qquad (2)$$

Two important differences in the stresses characteristics can be appreciated when comparing the stresses in the horizontal bulb turbine with the stresses measured in Kaplan and Francis turbines. In case of low head horizontal bulb turbines, the relative head variation with respect to the design point can be ±100%, while for Kaplan and specially Francis turbines this variation are much less important and so is the variation in the static stress [24, 25]. Regarding dynamic stresses, the analyzed tidal turbine does not show important variations in the full operating range. Note that this range is defined by the important variations in the operating net head. For Francis and Kaplan turbines, where the head is more constant and the operating point is adjusted by moving the wicket gates, the dynamic stresses show a great variation.

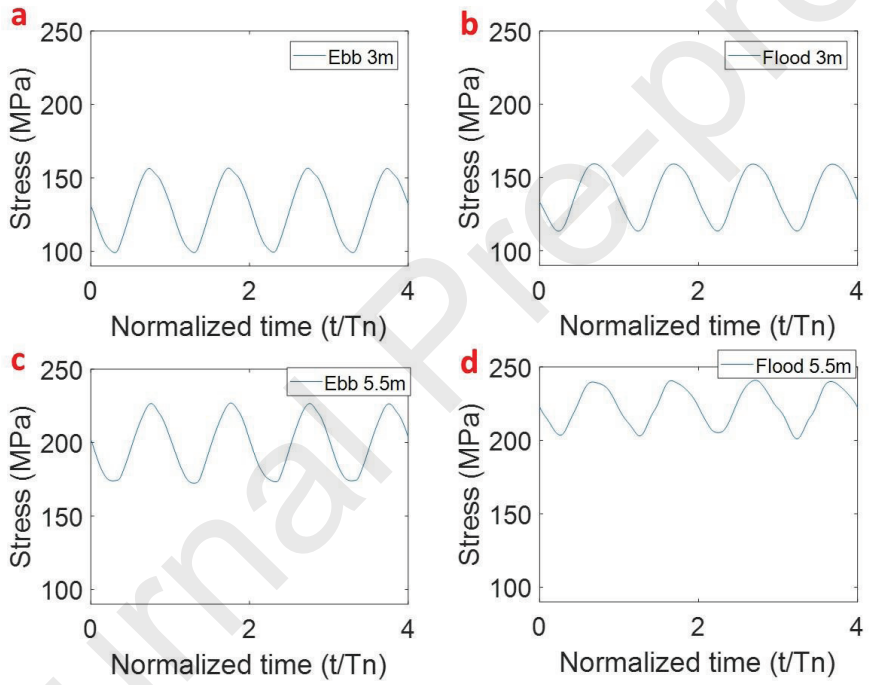

Figure 11: *Stress on the hotspot for a) Ebb mode and 3 m head b) Flood mode and 3 m head. c) Ebb mode and 5.5 m head d) Flood mode and 5.5 m head*

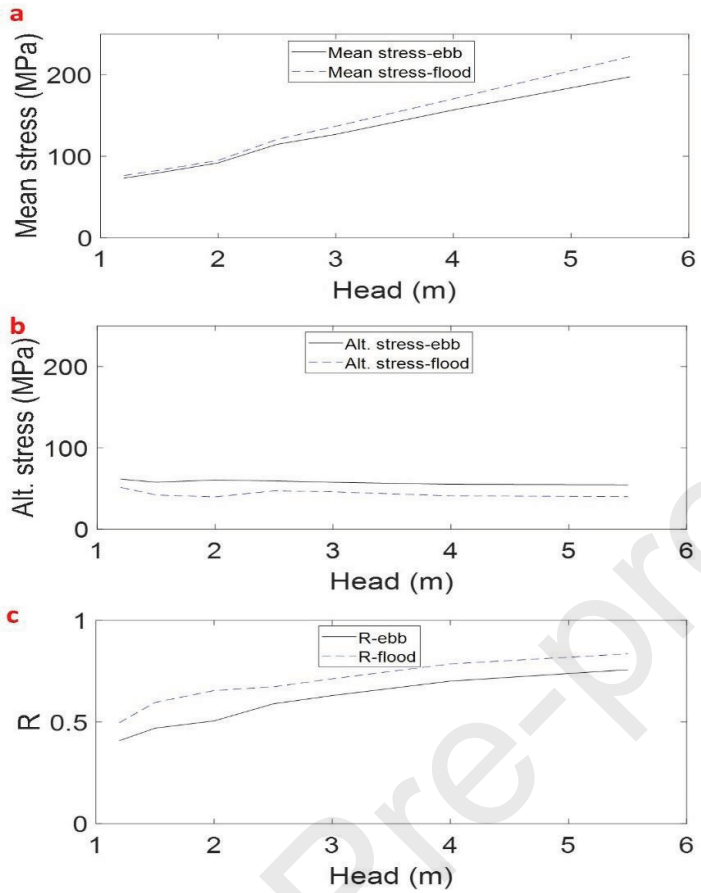

Figure 12: *a) Mean and b)alternating stress and c) R ratio as function of the head*

4. Fatigue analysis

Different fatigue and crack propagation models can be used to determine whether the crack will propagate or not and eventually calculate the number of cycles to failure. In context of hydropower, many researches use the Miner's rule to calculate the relative damage and useful life of every operating condition[27-29]. Gagnon et al.[34, 35] and Liu et al.[31] used a probabilistic approach to determine whether the crack will propagate or not. In this section we discuss the reliability of the turbine for the different operating modes and different heads considering the dynamic stresses and the fatigue limit.

4.1 Model without initial defect

First, we consider the static and dynamic stresses presented in the previous section. It is well known that the effect of the mean stresses on the S-N curve has to be considered and particularly for this material [39]. In fact, a tensile mean stress (positive mean value of stresses or $-1 < \mathrm{R} < 1$) shift the S-N curve reducing the fatigue limit, i.e. under these conditions less alternate stress is required to propagate the crack. For compressive mean stress the trend is opposite

The extensive studio of Lobato et al. [39] performed for this material show that the Goodman, Gerber or Kwofie's model are not adequate to describe the effects of the mean stress on the fatigue limit of the material. According to that study, the most adequate model is the Walker's model, where it is shown that the predictions based on this model fits the Basquin equation in the S-N curve. Taking into account

the results of that study, the fatigue limit can be obtained as a function of R. The data given in that study for different *R* and a quadratic regression adopted in this paper is represented in **Figure 13**.

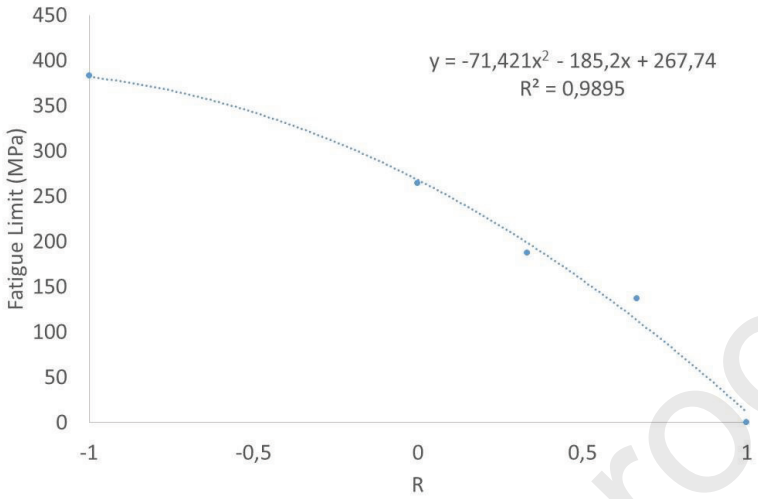

***Figure 13**: Fatigue limit (σ_f) as function of R*

Then, for every operating point the equivalent fatigue limit, considering the mean stress (R value) can be calculated. To determine whether the crack will or not propagate the fatigue limit is compared with the alternate stress for every condition. If the alternate stress is higher than the fatigue limit, then it is considered that the component will not last an infinite fatigue life and therefore the crack will propagate. **Figure 14** shows the alternate stress for the flood and ebb mode together with the corresponding fatigue limits obtained with the regression shown in **Figure 13** (fatigue limit depends on R).

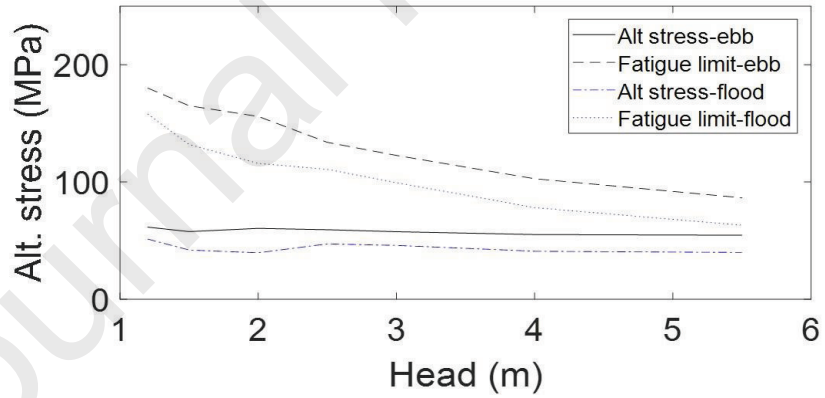

***Figure 14:** Alternate stress for ebb and flood mode and different heads. Corresponding fatigue limit*

As seen in this figure, for all the operating conditions the alternate stresses are below the respective fatigue limits and therefore, although for higher heads the alternate stresses are closer to the fatigue limit for both ebb and flood model, the crack should not propagate and the blades of the hydraulic turbine should last for an infinite life, which contradicts the experimental evidences found (**Figure 10**c).

4.2 Model with initial defect and reliability

As justified by many researchers, a realistic fatigue model should consider the possibility of the existence of an initial defect to explain and to analyze the mechanics of the crack propagation. In hydro

power, the works performed by Gagnon et al.[34, 35] and Liu et al.[31] consider the initial defect in a probabilistic way in order to analyze the reliability of hydropower components.

The modeling of the initial flaw with a Gumbel distribution with parameters $\mu = 1.5$ mm and $\beta = 0.5$ mm is justified in [31, 35, 40] for different types of hydraulic turbines. The probability of having an initial crack length smaller than a, can be then calculated according to the Gumbel cumulate distribution function:

$$F(a) = P(A < a) = e^{-e^{-\frac{(a-\mu)}{\beta}}} = e^{-e^{-\frac{(a-1.5)}{0.5}}} \quad (3)$$

Here, we briefly summarize the adoption of $\mu = 1.5$ mm and $\beta = 0.5$. With these parameters the cumulate function includes many non-observable but possible cases (very small defect sizes), excludes almost all physically impossible cases below 0 mm ($P(A < 0) \approx 0$) and excludes almost all large size defects where the defect would be detected and therefore repaired ($P(A > 3) \approx 0.05$). The reference value 3 mm is taken from [33], as a value where an initial crack can be detected and therefore repaired. The adoption of the Gumbel distribution in front of other models is justified because such distribution is an extreme value distribution, that represents the uncertainty for the largest initial defects in a group of many possible defects.

We introduce this defect on the critical section of the blade of the simulation model and recalculate the static and dynamic stresses. For this purpose, a small part of the material has been removed from the blade with the shape of a triangular crack front and the surrounding area has been remeshed with a finer mesh. This is shown in Figure 15.

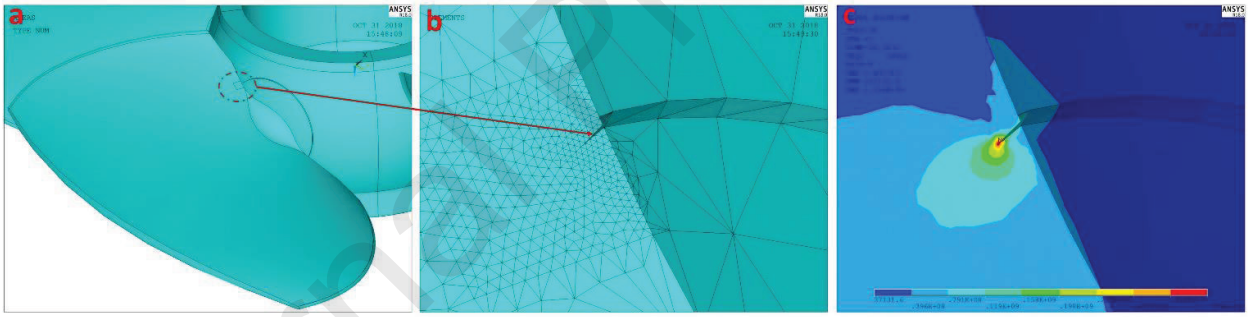

Figure 15: *Simulation model considering a crack. a) View of one blade b) Detail of the initial crack and remesh area c) Concentration of stresses on crack front*

By introducing a small crack, the static and dynamic stresses will increase due to stress concentration effect depending on the crack length[31]. Therefore, for every crack length the curves of the fatigue limit (which depends on the ratio R, Eq. (2)) and alternate stress are different (**Figure 14**). In order to determine the dependency of these two curves with the crack length with a number of reasonable simulations, we consider four different cracks with values 1.5mm, 2.5mm and 4mm. For these crack lengths, simulations for the Flood and Ebb mode operating with heads of 1.2m, 2.5m and 5.5m have been performed. This corresponds to the minimum head, an intermediate head and the maximum head of the range. For the different crack lengths, 4mm has been adopted as the larger value simulated, as $F(4) = 0.993$ (Eq.3) and therefore the probability of having a larger crack is less than 1%. The total number of conditions simulated including the crack length parameter is shown in **Table 2**.

Table 2: *Total of simulations performed including the parameter of the crack length*

Crack length	0 mm	1.5 mm	2.5 mm	4 mm
Head (m)	1.2, 1.5, 2, 2.5, 3, 4, 5.5	1.2, 2.5, 5.5	1.2, 2.5, 5.5	1.2, 2.5, 5.5
Modes	Ebb/ Flood	Ebb/ Flood	Ebb/ Flood	Ebb/ Flood

In this way, the static, dynamic stress, R coefficients and fatigue limits have been calculated for the conditions listed in **Table 2**. To obtain a continuous characteristic of alternate stress and fatigue limit the curves have been interpolated first for a constant crack length. Then to obtain the different curves as function of the crack length, a second interpolation has been performed. This procedure is illustrated in **Figure 16**, exemplified for the mean stress in ebb mode. The mean stress for the ebb mode with a crack length in the range of 0mm to 1.5mm can be calculated by interpolation of these two curves, which have been previously obtained with numerical simulation(**Table 2**). The same procedure can be performed to obtain the alternate stress, R and fatigue limit for any crack length.

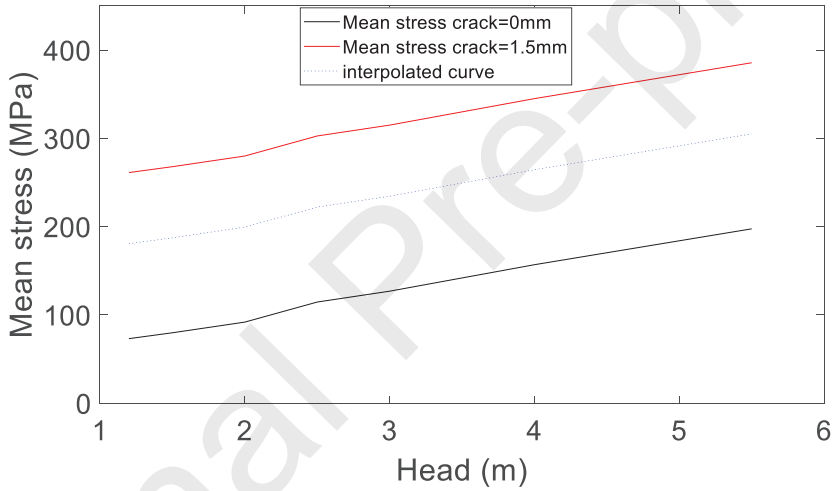

Figure 16: *Interpolation of a characteristic curve with the crack length*

The alternate stress and the fatigue limit can be then represented as a function of the crack length for every operating condition. As an example, **Figure 17** shows the evolution of the alternate stress and the fatigue limit for the Ebb mode and with a head of 2.5m. As the initial crack length increases, the mean and alternate stress increases, which is a coherent result with the Linear Elastic Fracture Mechanics theory. As the mean stresses increases also the R value increases and the fatigue limit decreases. For crack length=0 mm, the values of alternate stress and fatigue limit correspond to those ones presented in **Figure 14** for the Ebb mode and head 2.5m. In this point, as noticed in the previous section, the fatigue limit is over the alternate stress and therefore the unit works in a safe zone.

The critical crack length is defined then as the length, where the alternate stress overcome the fatigue limit. For the head represented in **Figure 17** (2.5 m) this happens for 1.68 mm. For larger crack lengths the fatigue limit is below the alternate stress and therefore the crack will propagate and the blade will not last an infinite life. In the same way, the critical crack length has been calculated for the rest of the operating heads simulated (**Table 2**).

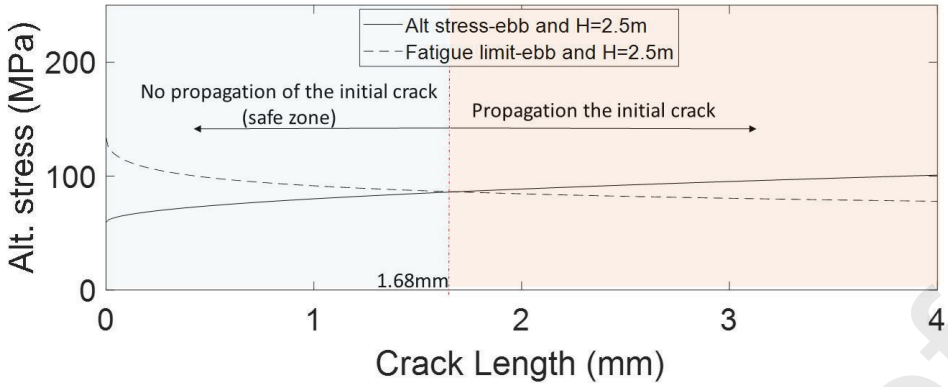

Figure 17: *Alternate stress and fatigue limit for the Ebb mode and H=2.5m. Influence of the initial crack length*

The probability of having a smaller crack than the critical one and therefore the probability that the initial crack will not propagate is obtained by means of the distribution model adopted, in this case the Gumbel distribution represented in Eq.(3). Therefore, it is reasonable to describe the reliability of the blade to last infinite life operating in this condition as exactly this probability, which can be calculated as:

$$Re_{H=2.5,Ebb\ mode}(\infty) = P(T > \infty) = P(A < a_{critical}) = P(A < 1.68) = e^{-e^{-\frac{(1.68-1.5)}{0.5}}} \quad (4)$$
$$= 0.4977 = 49.77\%$$

This value can be interpreted as follows: For the machine working with a head of 2.5 meters in the Ebb mode, in 49.77% of the installed blades (assuming symmetry of the blades, mounting conditions and same types of unit) the crack will not propagate and the blade will last an infinite life. We notice that according to the basic theory of reliability no system can last an infinite life. In the present case, infinite can be interpreted as a value higher than the limit represented in the S-N curve, which is usually around 10^9 cycles.

In the same way, the reliability to infinite life can be calculated for the rest of operating conditions, which are represented in **Figure 18**. This figure summarizes all the fatigue analysis performed in this paper. For low heads, a large initial crack for a further propagation is necessary, which is less probable to exist and therefore the reliability to infinite life is high (around 80% for the ebb mode and 70% for the flood mode). For heads larger than 2 meters there is an abrupt decrease of the reliability. For the highest head of the operating range (H=5.5m) the reliability to infinite life is almost 0, which means that working in this condition a small initial crack will propagate with a very high probability and therefore the blades will not last an infinite life.

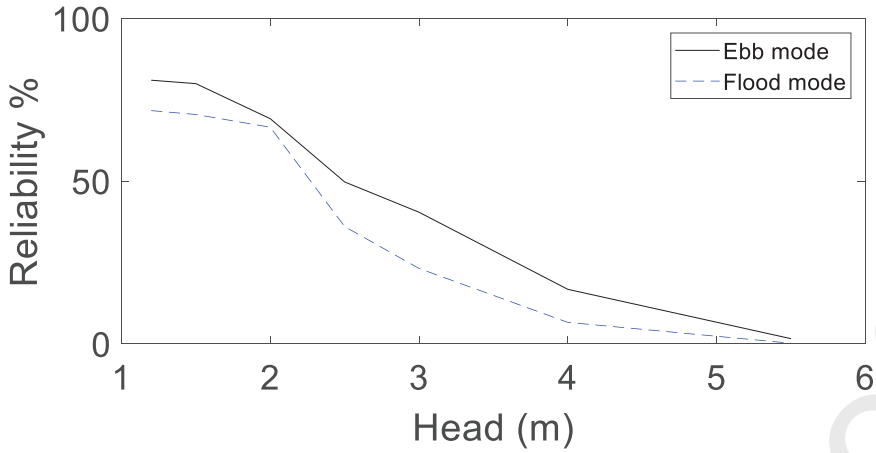

Figure 18: *Reliability to infinite life of the blades in the Ebb and Flood mode*

5. Conclusions

This paper analyzes the fatigue life of a low head bidirectional tidal turbine with the purpose of determining under which operating conditions the blades are more prone to develop cracks. Such studies have been widely performed for Francis and Kaplan turbines as the number of operating units is much larger, but not for tidal turbines due to the relative few number of existing machines. Nevertheless, many studies forecast a great increase of the exploitation of this type of renewable energy and therefore the conclusions of this study can be useful for further tidal turbine designs and fatigue life estimations.

Particularly, by means of a numerical FSI model including the flow simulation (CFD) coupled with a structural model (FEM) considering an initial defect, it has been shown that:

- For higher heads the reliability of the blades for an infinite life is very low, which implies that working in these operating conditions cracks are very likely to propagate and therefore many blades will not last an infinite life.
- The influence of the mean stresses, initial small defects on the fatigue limit and alternate stresses have to be considered in order to properly justify the propagation of the crack.
- The stress hotspot predicted with the numerical model coincides with the crack initiation point found in some blades of the prototype units. The main stress characteristics of such turbines greatly differs from those ones in Francis or Kaplan turbines, where mean and alternate stress greatly varies in all the operating range. In tidal turbines by changing the operating condition, mean stresses suffer from a great variation due to the head variation but the alternate stress remain approximately constant.
- The pressure and stress fluctuations on the blade can be explained with the relative variation of the static pressure due to the rotation of the blades around a horizontal shaft. Therefore, the main characteristic frequency component on the dynamic stress is the rotating frequency of the unit, which also differs from other higher head turbines dominated by the rotor stator interaction (RSI).

Acknowledgments

The authors thank the National Natural Science Foundation of China (No. 51779122, No. 51439002),

Tsinghua University Initiative Scientific Research Program (No. 20151080459), China Postdoctoral Science Foundation (No. 2018M631466) and the Jiangxia Tidal Test Power Station for supporting the present work.

References

[1] Rourke FO, Boyle F, Reynolds A. Tidal energy update 2009. Applied Energy. 2010;87:398-409.
[2] Clark RH. Elements of tidal-electric engineering: John Wiley & Sons; 2007.
[3] Charlier RH. Forty candles for the Rance River TPP tides provide renewable and sustainable power generation. Renewable and Sustainable Energy Reviews. 2007;11:2032-57.
[4] Bernshtein LB. Tidal power plants in Russia. IEEE Power Engineering Review. 1994;14:18.
[5] Power NS. Annapolis tidal power plant. 2009.
[6] Wang S, Yuan P, Li D, Jiao Y. An overview of ocean renewable energy in China. Renewable and Sustainable Energy Reviews. 2011;15:91-111.
[7] Cho YS, Lee JW, Jeong W. The Construction of a Tidal Power Plant at Sihwa Lake, Korea. Energy Sources, Part A: Recovery, Utilization, and Environmental Effects. 2012;34:1280-7.
[8] Ferreira RM, Estefen SF. Alternative concept for tidal power plant with reservoir restrictions. Renewable Energy. 2009;34:1151-7.
[9] Xia J, Falconer RA, Lin B. Impact of different operating modes for a Severn Barrage on the tidal power and flood inundation in the Severn Estuary, UK. Applied Energy. 2010;87:2374-91.
[10] Lee DS, Oh S-H, Yi J-H, Park W-S, Cho H-S, Kim D-G, et al. Experimental investigation on the relationship between sluice caisson shape of tidal power plant and the water discharge capability. Renewable Energy. 2010;35:2243-56.
[11] Bae YH, Kim KO, Choi BH. Lake Sihwa tidal power plant project. Ocean Engineering. 2010;37:454-63.
[12] Zhengwei W, Xiaosheng Y, Yexiang X. Hydraulic performance optimization of bidirectional tidal power turbine [J]. Journal of Drainage and Irrigation Machinery Engineering. 2010;5:417-21.
[13] Wang ZW, Luo YY, Zhou LJ, Xiao RF, Peng GJ. Computation of dynamic stresses in piston rods caused by unsteady hydraulic loads. Engineering Failure Analysis. 2008;15:28-37.
[14] Luo Y, Wang Z, Zeng J, Lin J. Fatigue of piston rod caused by unsteady, unbalanced, unsynchronized blade torques in a Kaplan turbine. Engineering Failure Analysis. 2010;17:192-9.
[15] Liu S, Li S, Wu Y. Pressure fluctuation prediction of a model Kaplan turbine by unsteady turbulent flow simulation. Journal of Fluids Engineering. 2009;131:101102.
[16] Trivedi C. Compressible Large Eddy Simulation of a Francis Turbine During Speed-No-Load: Rotor Stator Interaction and Inception of a Vortical Flow. Journal of Engineering for Gas Turbines and Power. 2018;140:112601--18.
[17] Mende C, Weber W, Seidel U. Progress in load prediction for speed-no-load operation in Francis turbines. IOP Conference Series: Earth and Environmental Science. 2016;49:062017.
[18] Morissette JF, Chamberland-Lauzon J, Nennemann B, Monette C, Giroux AM, Coutu A, et al. Stress predictions in a Francis turbine at no-load operating regime. IOP Conference Series: Earth and Environmental Science. 2016;49:072016.
[19] Yamamoto K, Mï¿½ller A, Favrel A, Landry C, Avellan F. Numerical and experimental evidence of the inter-blade cavitation vortex development at deep part load operation of a Francis turbine. IOP Conference Series: Earth and Environmental Science. 8 ed2016.
[20] Wang Z, Zhou L. Simulations and measurements of pressure oscillations caused by vortex ropes.

Journal of fluids engineering. 2006;128:649-55.
[21] Bouajila S, De Colombel T, Lowys P, Maitre T. Hydraulic Phenomena Frequency Signature of Francis Turbines Operating in Part Load Conditions. IOP Conference Series: Earth and Environmental Science: IOP Publishing; 2016. p. 082001.
[22] Huang X, Oram C, Sick M. Static and dynamic stress analyses of the prototype high head Francis runner based on site measurement. IOP Conference Series: Earth and Environmental Science. 2014;22:032052.
[23] Seidel U, Hübner B, Löfflad J, Faigle P. Evaluation of RSI-induced stresses in Francis runners. IOP Conference Series: Earth and Environmental Science. 2012;15:052010.
[24] Zhou L, Wang Z, Xiao R, Luo Y. Analysis of dynamic stresses in Kaplan turbine blades. Engineering computations. 2007;24:753-62.
[25] Xiao R, Wang Z, Luo Y. Dynamic Stresses in a Francis Turbine Runner Based on Fluid-Structure Interaction Analysis. Tsinghua Science & Technology. 2008;13:587-92.
[26] Egusquiza E, Valero C, Huang X, Jou E, Guardo A, Rodriguez C. Failure investigation of a large pump-turbine runner. Engineering Failure Analysis. 2012;23:27-34.
[27] Huang X, Chamberland-Lauzon J, Oram C, Klopfer A, Ruchonnet N. Fatigue analyses of the prototype Francis runners based on site measurements and simulations. IOP Conference Series: Earth and Environmental Science. 2014;22:012014.
[28] Seidel U, Mende C, Hübner B, Weber W, Otto A. Dynamic loads in Francis runners and their impact on fatigue life. IOP Conference Series: Earth and Environmental Science. 2014;22:032054.
[29] Monette C, Marmont H, Chamberland-Lauzon J, Skagerstrand A, Coutu A, Carlevi J. Cost of enlarged operating zone for an existing Francis runner. IOP Conference Series: Earth and Environmental Science. 2016;49:072018.
[30] Duparchy F, Brammer J, Thibaud M, Favrel A, Lowys P, Avellan F. Mechanical impact of dynamic phenomena in Francis turbines at off design conditions. Journal of Physics: Conference Series: IOP Publishing; 2017. p. 012035.
[31] Liu X, Presas A, Luo Y, Wang Z. Crack growth analysis and fatigue life estimation in the piston rod of a Kaplan hydro turbine. Fatigue and Fracture of Engineering Materials and Structures. 2018.
[32] Liu X, Luo YY, Wang ZW. Fatigue Analysis of the Piston Rod in a Kaplan Turbine Based on Crack Propagation under Unsteady Hydraulic Loads. IOP Conference Series: Earth and Environmental Science. 2014;22:012017.
[33] Gagnon M, Tahan A, Bocher P, Thibault D. Influence of load spectrum assumptions on the expected reliability of hydroelectric turbines: A case study. Structural Safety. 2014;50:1-8.
[34] Gagnon M, Tahan A, Bocher P, Thibault D. A probabilistic model for the onset of High Cycle Fatigue (HCF) crack propagation: Application to hydroelectric turbine runner. International Journal of Fatigue. 2013;47:300-7.
[35] Gagnon M, Tahan SA, Bocher P, Thibault D. The role of high cycle fatigue (HCF) onset in Francis runner reliability. IOP Conference Series: Earth and Environmental Science. 2012;15:022005.
[36] https://hyperbole.epfl.ch. HYdropower plants PERformance and flexiBle Operation towards Lean integration of new renewable Energies. 2013.
[37] Menter FR. Two-equation eddy-viscosity turbulence models for engineering applications. AIAA journal. 1994;32:1598-605.
[38] Bathe K-J. Finite element procedures: Klaus-Jurgen Bathe; 2006.
[39] da Silva BL, de Almeida Ferreira J, Oliveira F, Araújo J. Influence of mean stress on the fatigue

strength of ASTM A743 CA6NM alloy steel. Frattura ed Integrità Strutturale. 2010;4:17-26.
[40] Gagnon M, Tahan A, Bocher P, Thibault D. On the fatigue reliability of hydroelectric Francis runners. Procedia Engineering. 2013;66:565-74.

HIGHLIGHTS

- Fatigue analysis and useful life estimation of the blades of low head bidirectional tidal turbines have been discussed in this paper.
- The conclusions of these study could be contrasted with real cracks observed in prototypes.
- By means of a numerical FSI model including CFD coupled with structural model (FEM) and considering an initial defect, the most dangerous operating conditions for crack propagation in the blades have been determined and numerically quantified (reliability).
- Main characteristics of the pressure fluctuations and dynamic stresses in horizontal bulb turbines for tidal barrages have been determined and presented.

Declaration of interests

☒ The authors declare that they have no known competing financial interests or personal relationships that could have appeared to influence the work reported in this paper.

☐The authors declare the following financial interests/personal relationships which may be considered as potential competing interests: